An Extremum Seeking Algorithm based on Square Wave for Three-Dimensional Wireless Power Transfer System to Achieve Maximum Power Transmission

Hanbing Dan, *Member*, *IEEE*, Yuqian Chao, Guo Xu, *Member*, *IEEE*, Zixi Liu, Hua Han, Mei Su, *Member*, *IEEE*, Yao Sun, *Member*, *IEEE*

Abstract—This paper proposes an extremum seeking algorithm (ESA) based on square wave, which provides an alternative method to the dynamic maximum power transmission problem of the three-dimensional (3D) wireless power transfer (WPT) system. The proposed method uses square wave signal instead of sinusoidal signal as the detection signal, which is simpler to implement in the discrete control system. By simultaneously detecting two azimuths of the 3D WPT system, the detection time of the maximum power transmission point is reduced. The convergence of the ESA based on square wave is verified according to the mathematical model of the system. Finally, an experiment prototype is set up to verify the correction and effectiveness of the ESA based on square wave. The experiment results manifest that the system can reach the maximum power transmission point within 150ms after the load position varies.

***Index Terms*—Three-dimensional WPT, load tracking, maximum power transmission, extremum seeking, square wave**

I. Introduction

WPT technology has attracted great attention since it was proposed by Tesla in 1893[1]. The commonly used WPT method is the magnetic field coupling method [2], [3]. And because of the convenience and safety of magnetic field coupling WPT system, it has been widely used in electric vehicles [4]-[6], smart phones [7], medical implants [8], [9], and autonomous underwater vehicle [10], etc. However, the position robustness of wireless power devices used in daily life is poor. And WPT system with longer transmission distance and higher spatial freedom is urgently needed.

To allow the WPT system have better location robustness, various methods have been proposed to improve the performance of the magnetic field coupling WPT system. For example, megahertz operation frequency [11], [12], addition of relay coils [13], [14] and design of multiple coils [15]-[18]. However, megahertz operation frequency and addition of relay coils can only enhance the position robustness of the system within a certain range. Therefore, in order to transmit power to loads in any orientation, the commonly used method is the design of multiple coils.

In order to achieve more robust wireless power transmission, a novel wireless charging bowl with multiple transmitter coils is proposed to provide power for portable devices [19]. When the load equipment is at any position in the bowl, the wireless power transmission system can achieve higher efficiency. However, the device can only charge the devices in the bowl, and cannot achieve omnidirectional wireless power transfer outside the bowl.

The load equipment may exist in any position in space instead of a specific direction, so the research on omnidirectional WPT becomes extremely important. To realize the omnidirectional wireless power transfer, the two-dimensional and three-dimensional WPT system based on the structure of an orthogonal circular coil is proposed [20]-[22]. The general principle of load detection is explained based on the mathematical model of the system. However, the proposed load detection method is complicated and not suitable for the occasion that the load location changes.

In order to achieve dynamic load tracking of a two-dimensional WPT system with intermittent moving and frequent moving equipment, two different maximum power transmission methods based on parameter identification and gradient descent are proposed, respectively [23]. It realizes the maximum power transmission in most directions except when the load is directly above or below the two-dimensional WPT system. To solve this problem, a dynamic load tracking method of 3D WPT system based on gradient descent algorithm is proposed [24]. However, it requires to separately detect the two azimuth angles step by step to determine the load position, which is complicated and computationally intensive.

To address this issue, this paper proposes an ESA based on square wave, which can simply realize load detection and achieve efficient power transmission in 3D WPT system. The

Manuscript received March 9, 2021; revised June 15, 2021; accepted July 19, 2021. This work was supported by the Hunan Provincial Key Laboratory of Power Electronics Equipment and Grid under Grant 2018TP1001, in part by the National Natural Science Foundation of China under Grant 61903382, 51907206, 61933011, in part by the Natural Science Foundation of Hunan Province, China under Grant 2020JJ5722. (Corresponding Author: Guo Xu)

H. Dan, Y. Chao, G. Xu, Z. Liu, H. Han, M. Su, Y. Sun are with the school of automation, Central South University, Changsha 410012, China (daniel698@sina.cn, chaoyuqian@csu.edu.cn, xuguocsu@csu.edu.cn, zgliuzixi@163.com, hua_han@126.com, sumeicsu@mail.csu.edu.cn, yaosuncsu@gmail.com).

traditional ESA [25], [26] can achieve mutual non-interference in the searching process through the frequency separation of its detection signals. By simultaneously detecting two azimuths of the 3D WPT system, the optimization process can be accelerated. However, the detection signal of the traditional ESA is a sinusoidal waveform, and achieving continuous high frequency time-varying current control is difficult in the discrete control system. Therefore, an ESA based on square wave that uses the square wave instead of the sine wave as the detection signal is proposed, which is simple to implement in the discrete control system.

The rest of this paper is organized as follows: In section II, the circuit model and mathematical model of the 3D WPT system are introduced. In section III, the principle of maximum power transmission is introduced. In section IV, the implementation steps of the ESA based on square wave to achieve the maximum power transmission are introduced, and the convergence of the system is analyzed. In section V, the previous algorithm is verified and analyzed by experiments. In section VI, different load tracking methods are analyzed and compared. In section VII, a conclusion is drawn. The first-order partial derivative and the second-order partial derivative of the objective function of maximum power transmission are verified in the Appendix.

II. Structure and Mathematical Model of 3D WPT System

A. Structure of the 3D WPT System

The three-dimensional WPT system includes three mutually orthogonal transmitting coils and one receiving coil. The basic structure is shown in Fig. 1. Compared with the traditional planar WPT system, its transmission distance is longer, the location robustness is stronger. Thus, it is more flexible for the 3D WPT system to adapt the scenarios where the load moves. Each transmitting part is composed of three parts: H-bridge inverter, resonance compensation capacitor and coil. The receiving part is also composed of load resistance, resonance compensation capacitor and coil.

Compared with the traditional WPT system, the biggest advantage of the three-dimensional WPT system is that it can shape the magnetic field. The direction of the synthesized magnetic field vector can be controlled by adjusting the currents flowing through the three transmitting coils. If the magnetic field vector can be controlled to point to the load position, then more efficient energy transmission can be achieved.

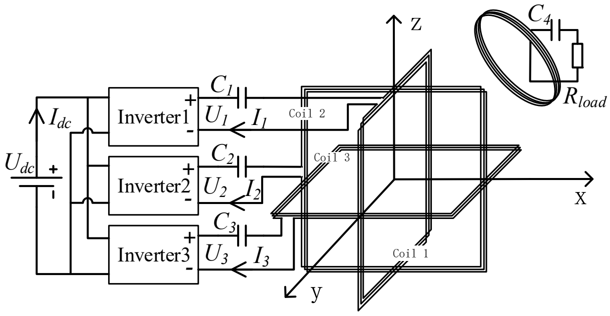

Fig. 1. Three-orthogonal coil structure of the 3D WPT system

B. Circuit Model of the 3D WPT System

In this paper, DC low-voltage power supply is used, and the ideal DC voltage source is transformed into a controllable AC voltage output by controlling the H-bridge inverter. Since the output voltage of the inverter is a square wave, a series LC resonant circuit network is connected to obtain the desired sinusoidal current. And the output currents of the H-bridge inverters are controlled by phase shift control [27]. The series LC resonant circuit network is composed of a resonant compensation capacitor and a transmitting coil. Since it is necessary to control the current flowing through the three coils separately, three H-bridge inverters are used. The circuit model of the whole system is shown in Fig. 2.

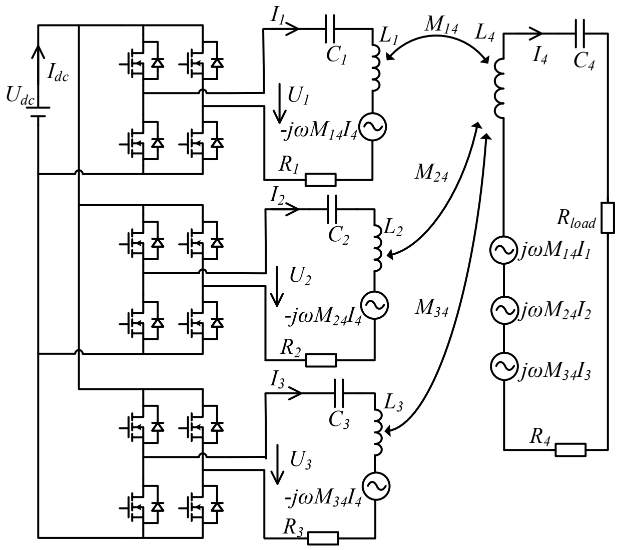

Fig. 2. The circuit model for a 3D WPT system

Fig. 2 illustrates the coupling relationship between the three transmitting coils and the receiving coils of the three-dimensional WPT system. U_{dc} and I_{dc} are the output voltage and current of the DC voltage source. U_1, U_2, U_3 are the output voltage of the three inverters respectively. I_1, I_2, I_3, and I_4 are the currents of the three transmitting coils and the current flowing through the receiving coil respectively.

C_1, C_2, C_3, C_4 are the resonant compensation capacitors of the three transmitting coil resonant circuits and one receiving coil resonant circuit. L_1, L_2, L_3, L_4 are the inductances of the three transmitting coils and the receiving coil. R_1, R_2, R_3, R_4 are the internal resistances of the three transmitting coils and the receiving coil. R_{load} is the load resistance. M_{14}, M_{24} and M_{34} are the mutual inductance between the transmitting coils and the receiving coil.

C. Mathematical Model of the 3D WPT System

In Fig. 3, the magnetic field vector $\vec{F}$ is synthesized by the basic magnetic field vectors $\vec{f_1}, \vec{f_2}$ and $\vec{f_3}$ generated by three transmitting coils. As the magnitude of $\vec{f_1}$, $\vec{f_2}$ and $\vec{f_3}$ are proportional to these currents, the magnetic field vector $\vec{F}$ can be adjusted by controlling the current flowing through the three transmitting coils. The relationship between the direction of the synthesized magnetic field vector and the current of the three coils can be expressed as

$$\begin{bmatrix} \mathbf{I}_1 \\ \mathbf{I}_2 \\ \mathbf{I}_3 \end{bmatrix} = \begin{bmatrix} \sin\theta\cos\varphi \\ \sin\theta\sin\varphi \\ \cos\theta \end{bmatrix} I \tag{1}$$

where $\mathbf{I}_1, \mathbf{I}_2, \mathbf{I}_3$ are the currents flowing through the three coils, and I is a sinusoidal time function [21]. θ and φ are the azimuth angles of the synthesized magnetic field vector in the spherical coordinate system, as shown in Fig. 3.

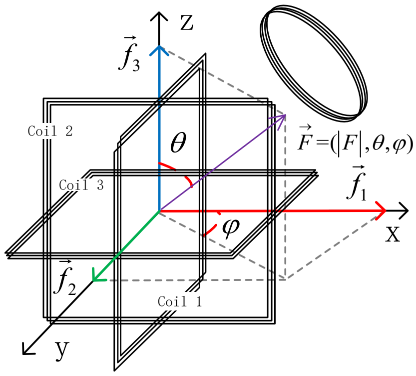

Fig. 3. Three orthogonal coil structure of 3D WPT system

The circuit model shown in Fig. 2 can be expressed as (2).

$$\begin{bmatrix} \mathbf{U}_1 \\ \mathbf{U}_2 \\ \mathbf{U}_3 \\ 0 \end{bmatrix} = \begin{bmatrix} R_1 + jX_1 & j\omega M_{12} & j\omega M_{13} & j\omega M_{14} \\ j\omega M_{12} & R_2 + jX_2 & j\omega M_{23} & j\omega M_{24} \\ j\omega M_{13} & j\omega M_{23} & R_3 + jX_3 & j\omega M_{34} \\ j\omega M_{14} & j\omega M_{24} & j\omega M_{34} & R_4 + R_{\text{load}} + jX_4 \end{bmatrix} \begin{bmatrix} \mathbf{I}_1 \\ \mathbf{I}_2 \\ \mathbf{I}_3 \\ \mathbf{I}_4 \end{bmatrix} \tag{2}$$

where: $X_1 = \omega L_1 - 1/\omega C_1$, $X_2 = \omega L_2 - 1/\omega C_2$,

$X_3 = \omega L_3 - 1/\omega C_3$, $X_4 = \omega L_4 - 1/\omega C_4$.

Since the three coils on the transmitting end are orthogonal to each other, $M_{12} = M_{13} = M_{23} = 0$. Substituting (1) into (2), the following equation (3) can be obtained by mathematical operation.

$$\begin{bmatrix} \mathbf{U}_1 \\ \mathbf{U}_2 \\ \mathbf{U}_3 \\ 0 \end{bmatrix} = \begin{bmatrix} Z_1 & 0 & 0 & j\omega M_{14} \\ 0 & Z_2 & 0 & j\omega M_{24} \\ 0 & 0 & Z_3 & j\omega M_{34} \\ j\omega M_{14} & j\omega M_{24} & j\omega M_{34} & Z_4 \end{bmatrix} \begin{bmatrix} I\sin\theta\cos\varphi \\ I\sin\theta\sin\varphi \\ I\cos\theta \\ \mathbf{I}_4 \end{bmatrix} \tag{3}$$

where: $Z_1 = R_1 + jX_1$, $Z_2 = R_2 + jX_2$, $Z_3 = R_3 + jX_3$, $Z_4 = R_4 + R_{load} + jX_4$.

III. Maximum Power Transmission Principle of 3D WPT System

The maximum power transmission of the 3D WPT system means that the energy received by the load resistance is the largest. To calculate the power consumed on the load resistor, the current flowing through the load resistor is obtained firstly. Expand and simplify the last line of equation (3) can get (4).

$$\begin{aligned} \mathbf{I}_4 = & -\frac{j\omega I}{R_4 + R_{load} + jX_4} \\ & \times(M_{14}\sin\theta\cos\varphi + M_{24}\sin\theta\sin\varphi + M_{34}\cos\theta) \end{aligned} \tag{4}$$

The power consumed by the load resistance of the receiving coil can be expressed as

$$P_{\text{load}} = I_4^{\ 2} R_{load} \tag{5}$$

where I_4 is the root mean square (RMS) value of $\mathbf{I}_4$.

Substituting (4) into (5), the load power can be simplified as

$$\begin{aligned} P_{\text{load}} = & \frac{\omega^2 I^2 R_{load}}{(R_4 + R_{load})^2 + X_4^{\ 2}} \times ((M_{14}^{\ 2} + M_{24}^{\ 2}) \\ & \times \sin^2(\arctan\frac{M_{14}}{M_{24}} + \varphi) + M_{34}^{\ 2})\sin^2(\gamma_{3-D} + \theta) \\ = & I^2 R_{load} K_{3-D}(\varphi)\sin^2(\gamma_{3-D} + \theta) \end{aligned} \tag{6}$$

where

$$K_{3-D}(\varphi) = \frac{\omega^2\left((M_{14}^{\ 2} + M_{24}^{\ 2})\sin^2(\arctan\frac{M_{14}}{M_{24}} + \varphi) + M_{34}^{\ 2}\right)}{(R_4 + R_{load})^2 + X_4^{\ 2}} \tag{7}$$

$$\gamma_{3-D} = \arctan\frac{M_{34}}{\sqrt{M_{14}^{\ 2} + M_{24}^{\ 2}}\sin(\arctan\frac{M_{14}}{M_{24}} + \varphi)} \tag{8}$$

In order to improve the system performance when achieving maximum power transmission, the efficiency of the system is considered. The efficiency of the system can be calculated from the load power and the total input power of the system. The total input power of the system is the sum of the power obtained by the load resistance and the system loss.

Since the system works in a fully resonant state, the main power loss of the system is the internal resistance of the four coils. Assuming that the internal resistances of the four coils are equal ($R_1 = R_2 = R_3 = R_4 = R$), the total input power of the system can be expressed as

$$\begin{aligned} P_{in} &= I^2 R_1 \sin^2\theta \cos^2\varphi + I^2 R_2 \sin^2\theta \sin^2\varphi \\ &+ I^2 R_3 \cos^2\theta + I_4^{\,2} R_4 + I_4^{\,2} R_{load} \\ &= I^2 R + I^2 (R_4 + R_{load}) K_{3-D}(\varphi) \sin^2(\gamma_{3-D} + \theta) \end{aligned} \tag{9}$$

The efficiency of the system is the ratio of the power consumed by the load resistance to the total input power, which can be expressed as

$$\begin{aligned} \eta &= \frac{P_{load}}{P_{in}} = \frac{I^2 R_{load} K_{3-D}(\varphi)\sin^2(\gamma_{3-D}+\theta)}{I^2 R + I^2 (R_4 + R_{load}) K_{3-D}(\varphi)\sin^2(\gamma_{3-D}+\theta)} \\ &= \frac{R_{load}}{\dfrac{R}{K_{3-D}(\varphi)\sin^2(\gamma_{3-D}+\theta)} + (R_4 + R_{load})} \end{aligned} \tag{10}$$

When the load position is determined, the variables in equations (6), (7), (8), (9), (10) are only θ and φ. According to (6), (9) and (10), the load power, the total input power and the efficiency will reach the maximum values at the same time when $K_{3-D}(\varphi)\sin^2(\gamma_{3-D}+\theta)$ gets the maximum value. According to (7) and (8), when $\sin^2(\arctan M_{14}/M_{24}+\varphi)=1$ and $\sin^2(\gamma_{3-D}+\theta)=1$, $K_{3-D}(\varphi)\sin^2(\gamma_{3-D}+\theta)$ will reach the maximum value. Thus, the conditions for the load power, the total input power and the efficiency to reach their maximum value is the same, and it can be expressed as

$$\begin{cases} \arctan\dfrac{M_{14}}{M_{24}} + \varphi = \dfrac{\pi}{2} \text{ or } \dfrac{3\pi}{2} \\ \gamma_{3-D} + \theta = \dfrac{\pi}{2} \text{ or } \dfrac{3\pi}{2} \end{cases} \tag{11}$$

IV. Realization of Maximum Power Transmission

A. Selection of Objective Function

The purpose of achieving maximum power transmission is to maximize the power received by the load resistance. And the total input power and the efficiency reach the maximum values at the same time. Therefore, maximizing the input power is chosen as the optimization aim because the input power can be easily measured at the transmitting end. The mutual inductance value in (11) is variable and unknown. It is clear that the optimal θ and φ should be determined to maximize the objective function. The objective function can be expressed as

$$f(\theta,\varphi) = P_{in} = I^2 R + I^2 (R_4 + R_{load}) K_{3-D}(\varphi)\sin^2(\gamma_{3-D}+\theta) \tag{12}$$

B. ESA based on Square Wave

The ESA based on square wave is designed for dynamic optimization target tracking, and the block diagram is shown in Fig. 4. First, an objective function is introduced, and the output of the multiplier can be considered as the gradient of the objective function. Changing the objective function along the positive gradient direction can easily maximize the objective function.

$q_1(t)$ and $q_2(t)$ in Fig. 4 are two square wave signals with different frequencies. After Fourier transformation, they can be expressed as (13) and (14). ω_1 and ω_2 are the corner frequencies of square wave signals $q_1(t)$ and $q_2(t)$ respectively and $\omega_2 \neq (2k+1)\omega_1$ (k=1, 2, 3, ……). Therefore, $\omega_2=2\omega_1$ is set in this paper.

$$q_1(t) = \sum \frac{1}{i}\sin(i\omega_1 t),\ i = 1,3,5,\cdots \tag{13}$$

$$q_2(t) = \sum \frac{1}{j}\sin(j\omega_2 t),\ j = 1,3,5,\cdots \tag{14}$$

$\hat{\theta}$ and $\hat{\varphi}$ are the estimated values of the azimuth angles θ and φ. $f(\theta,\varphi)$ is the objective function. h_1 and h_2 are the cutoff frequencies of the High-pass filter 1 and the High-pass filter 2, which are generally designed according to the principle $h_1=h_2 \le \omega_1$. k_1 and k_2 are the gains of the two integrators, respectively. a_1 and a_2 are the gains of the two detection signals, respectively. And the system convergence speed to the maximum point can be adjusted by k_1, k_2 and a_1, a_2. However, the growth of a_1 and a_2 will cause an increase in the steady-state error of the system.

The azimuth angle input is the sum of the estimate angles

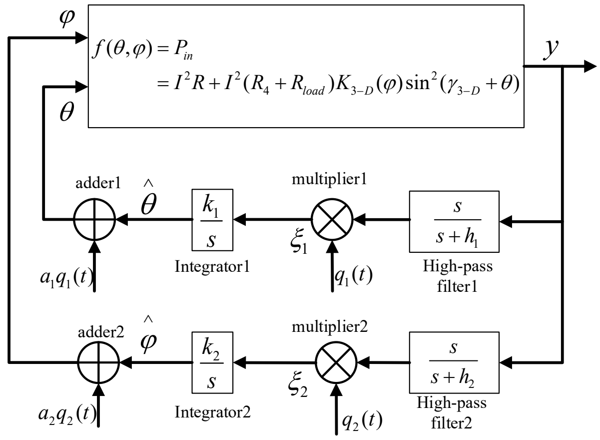

Fig. 4. Block diagram of ESA based on square wave for load tracking to achieve maximum power transmission

This article has been accepted for publication in a future issue of this journal, but has not been fully edited. Content may change prior to final publication. Citation information: DOI 10.1109/TIA.2021.3099777, IEEE Transactions on Industry Applications

$\hat{\theta}$ and $\hat{\varphi}$ and the detection signal $a_1 q_1(t)$ and $a_2 q_2(t)$. Each azimuth angle input corresponds to a power output. After the power output passes through a specific high-pass filter and multiplier, only the specific frequency signal is retained. Therefore, the working process of the two detecting loops will not affect each other through the frequency separation of the two search variables.

The ESA based on square wave shown in Fig. 4 includes two loops, which are the optimization processes of the azimuth angles θ and φ. The optimization goal is to make the estimation errors of the two search variables $\tilde{\theta}$ and $\tilde{\varphi}$ tend to 0, and the final search variable tends to the maximum point (θ^*, φ^*).

C. Convergence Analysis of the ESA based on Square Wave

Perform Taylor expansion of the objective function (12) at its maximum point (θ^*, φ^*) and ignore the higher-order terms to get (15).

$$\begin{aligned} f(\theta,\varphi) &= f(\theta^*,\varphi^*) + (\theta-\theta^*) f_\theta' + (\varphi-\varphi^*) f_\varphi' \\ &+ \frac{1}{2}[(\theta-\theta^*)^2 f_{\theta\theta}'' + (\varphi-\varphi^*)^2 f_{\varphi\varphi}'' \\ &+ (\theta-\theta^*)(\varphi-\varphi^*) f_{\theta\varphi}'' + (\theta-\theta^*)(\varphi-\varphi^*) f_{\varphi\theta}''] \end{aligned} \tag{15}$$

where $f_\theta' = \frac{\partial f(\theta,\varphi)}{\partial\theta}\Big|_{\theta=\theta^*}$, $f_\varphi' = \frac{\partial f(\theta,\varphi)}{\partial\varphi}\Big|_{\varphi=\varphi^*}$,

$$f_{\theta\theta}'' = \frac{\partial^2 f(\theta,\varphi)}{\partial\theta^2}\Bigg|_{\substack{\theta=\theta^*\\ \varphi=\varphi^*}},\ f_{\varphi\varphi}'' = \frac{\partial^2 f(\theta,\varphi)}{\partial\varphi^2}\Bigg|_{\substack{\theta=\theta^*\\ \varphi=\varphi^*}},$$

$$f_{\theta\varphi}'' = \frac{\partial^2 f(\theta,\varphi)}{\partial\theta\,\partial\varphi}\Bigg|_{\substack{\theta=\theta^*\\ \varphi=\varphi^*}},\ f_{\varphi\theta}'' = \frac{\partial^2 f(\theta,\varphi)}{\partial\varphi\,\partial\theta}\Bigg|_{\substack{\theta=\theta^*\\ \varphi=\varphi^*}}$$

Substituting (A12) into (15), the objective function can be simplified to

$$f(\theta,\varphi) = f(\theta^*,\varphi^*) + \frac{1}{2}[(\theta-\theta^*)^2 f_{\theta\theta}'' + (\varphi-\varphi^*)^2 f_{\varphi\varphi}''] \tag{16}$$

Set estimation errors: $\tilde{\theta} = \theta^* - \hat{\theta}$, $\tilde{\varphi} = \varphi^* - \hat{\varphi}$. It can be seen from Fig. 4: $\theta = \hat{\theta} + a_1 \sin(\omega_1 t)$, $\varphi = \hat{\varphi} + a_2 \sin(\omega_2 t)$. Substituting the above formula into (16), the following equation can be obtained by mathematical operation.

$$\begin{aligned} f(\theta,\varphi) &= f(\theta^*,\varphi^*) + \frac{1}{2}\left[(a_1 q_1(t) - \tilde{\theta})^2 f_{\theta\theta}'' + (a_2 q_2(t) - \tilde{\varphi})^2 f_{\varphi\varphi}''\right] \\ &= f(\theta^*,\varphi^*) + \frac{\tilde{\theta}^2}{2} f_{\theta\theta}'' + \frac{\tilde{\varphi}^2}{2} f_{\varphi\varphi}'' + \frac{a_1^2 q_1^2(t)}{2} f_{\theta\theta}'' \\ &+ \frac{a_2^2 q_2^2(t)}{2} f_{\varphi\varphi}'' - a_1 q_1(t)\tilde{\theta} f_{\theta\theta}'' - a_2 q_2(t)\tilde{\varphi} f_{\varphi\varphi}'' \end{aligned} \tag{17}$$

The output $f(\theta,\varphi)$ after filtering the DC signal through the high-pass filter can be expressed as

$$\begin{aligned} \frac{s}{s+h_1}[f(\theta,\varphi)] &= \frac{a_1^2 q_1^2(t)}{2} f_{\theta\theta}'' + \frac{a_2^2 q_2^2(t)}{2} f_{\varphi\varphi}'' \\ &- a_1 q_1(t)\tilde{\theta} f_{\theta\theta}'' - a_2 q_2(t)\tilde{\varphi} f_{\varphi\varphi}'' \end{aligned} \tag{18}$$

$$\begin{aligned} \frac{s}{s+h_2}[f(\theta,\varphi)] &= \frac{a_1^2 q_1^2(t)}{2} f_{\theta\theta}'' + \frac{a_2^2 q_2^2(t)}{2} f_{\varphi\varphi}'' \\ &- a_1 q_1(t)\tilde{\theta} f_{\theta\theta}'' - a_2 q_2(t)\tilde{\varphi} f_{\varphi\varphi}'' \end{aligned} \tag{19}$$

The output of High-pass filter 1 and High-pass filter 2 are multiplied by $q_1(t)$ and $q_2(t)$ respectively for demodulation and can be expressed as

$$\begin{aligned} \xi_1 &= q_1(t)\frac{s}{s+h_1}[f(\theta,\varphi)] \\ &= q_1(t)\frac{a_1^2 q_1^2(t)}{2} f_{\theta\theta}'' + q_1(t)\frac{a_2^2 q_2^2(t)}{2} f_{\varphi\varphi}'' \\ &- a_1 q_1^2(t)\tilde{\theta} f_{\theta\theta}'' - a_2 q_1(t) q_2(t)\tilde{\varphi} f_{\varphi\varphi}'' \end{aligned} \tag{20}$$

$$\begin{aligned} \xi_2 &= q_2(t)\frac{s}{s+h_2}[f(\theta,\varphi)] \\ &= q_2(t)\frac{a_1^2 q_1^2(t)}{2} f_{\theta\theta}'' + q_2(t)\frac{a_2^2 q_2^2(t)}{2} f_{\varphi\varphi}'' \\ &- a_1 q_1(t) q_2(t)\tilde{\theta} f_{\theta\theta}'' - a_2 q_2^2(t)\tilde{\varphi} f_{\varphi\varphi}'' \end{aligned} \tag{21}$$

Because of $\omega_2 \neq (2k+1)\omega_1$, DC signal only exists in $q_1^2(t)$ and $q_2^2(t)$. And expanded $q_1^2(t)$ in (20) can be expressed as

$$\begin{aligned} q_1^2(t) &= \sum \frac{1}{i_1}\sin(i_1\omega_1 t)\cdot\sum\frac{1}{i_2}\sin(i_2\omega_1 t) \\ &= \sum\frac{1}{2i_1 i_2}\left[\cos[(i_1-i_2)\omega_1 t] - \cos[(i_1+i_2)\omega_1 t]\right] \\ & i_1 = 1,3,5,\cdots,\ i_2 = 1,3,5,\cdots \end{aligned} \tag{22}$$

Separate case $i_1 = i_2 = n$ from case $i_1 \neq i_2$, equation (22) can be expressed as

$$\begin{aligned} q_1^2(t) &= \sum\frac{1}{2n^2}[1-\cos(2n\omega_1 t)] \quad (i_1 = i_2 = n) \\ &+ \sum\frac{1}{2i_1 i_2}\left[\cos[(i_1-i_2)\omega_1 t] - \cos[(i_1+i_2)\omega_1 t]\right] \quad (i_1 \neq i_2) \end{aligned} \tag{23}$$

Similarly, $q_2^2(t)$ can be expressed as

$$\begin{aligned} q_2^2(t) &= \sum\frac{1}{2n^2}[1-\cos(2n\omega_2 t)] \quad (j_1 = j_2 = n) \\ &+ \sum\frac{1}{2j_1 j_2}\left[\cos[(j_1-j_2)\omega_2 t] - \cos[(j_1+j_2)\omega_2 t]\right] \quad (j_1 \neq j_2) \end{aligned} \tag{24}$$

After the AC signal is filtered by the integrator, its output can be expressed as

This article has been accepted for publication in a future issue of this journal, but has not been fully edited. Content may change prior to final publication. Citation information: DOI 10.1109/TIA.2021.3099777, IEEE Transactions on Industry Applications

$$\frac{k_1}{s}[\xi_1] \approx \frac{k_1}{s}[-\sum \frac{1}{2n_1^{\,2}} a_1 \tilde{\theta} f_{\theta\theta}'']\tag{25}$$

$$\frac{k_2}{s}[\xi_2] \approx \frac{k_2}{s}[-\sum \frac{1}{2n_2^{\,2}} a_2 \tilde{\varphi} f_{\varphi\varphi}'']\tag{26}$$

Because $\sum \frac{1}{2n^2}$ is a gain and does not affect the final result, it can be ignored. Therefore, the estimated values of θ and φ can be expressed as

$$\hat{\theta} = \frac{k_1}{s}[-\frac{a_1 f_{\theta\theta}''}{2}\tilde{\theta}]\tag{27}$$

$$\hat{\varphi} = \frac{k_2}{s}[-\frac{a_2 f_{\varphi\varphi}''}{2}\tilde{\varphi}]\tag{28}$$

The partial derivatives of the estimated values of $\hat{\theta}$ and $\hat{\varphi}$ can be expressed as

$$\hat{\theta}' = -\frac{a_1 k_1 f_{\theta\theta}''}{2}\tilde{\theta}\tag{29}$$

$$\hat{\varphi}' = -\frac{a_2 k_2 f_{\varphi\varphi}''}{2}\tilde{\varphi}\tag{30}$$

After some mathematical operation, the partial derivatives of the estimated errors $\tilde{\theta}$ and $\tilde{\varphi}$ are expressed as

$$\tilde{\theta}' = -\hat{\theta}' = \frac{a_1 k_1 f_{\theta\theta}''}{2}\tilde{\theta} = \frac{a_1 k_1 f_{\theta\theta}''}{2}(\theta^* - \hat{\theta})\tag{31}$$

$$\tilde{\varphi}' = -\hat{\varphi}' = \frac{a_2 k_2 f_{\varphi\varphi}''}{2}\tilde{\varphi} = \frac{a_2 k_2 f_{\varphi\varphi}''}{2}(\varphi^* - \hat{\varphi})\tag{32}$$

In the above equations (31) and (32), a_1, a_2, k_1, k_2 are all positive numbers, and $f_{\theta\theta}''$, $f_{\varphi\varphi}''$ are negative numbers (the second derivative of the function at its maximum point is negative). Therefore, the condition for convergence can be obtained as

$$\tilde{\theta}\cdot\tilde{\theta}' = \frac{a_1 k_1 f_{\theta\theta}''}{2}\tilde{\theta}^2 \le 0\tag{33}$$

$$\tilde{\varphi}\cdot\tilde{\varphi}' = \frac{a_2 k_2 f_{\varphi\varphi}''}{2}\tilde{\varphi}^2 \le 0\tag{34}$$

Therefore, through the iteration of ESA, the estimation error of the azimuth angle of the synthesized magnetic field vector tends to zero. The system will eventually converge to the maximum power transmission point.

V. Experimental Verification

In order to verify the correctness of the previous analysis, an experimental prototype of the 3D WPT system was built, as shown in Fig. 5.

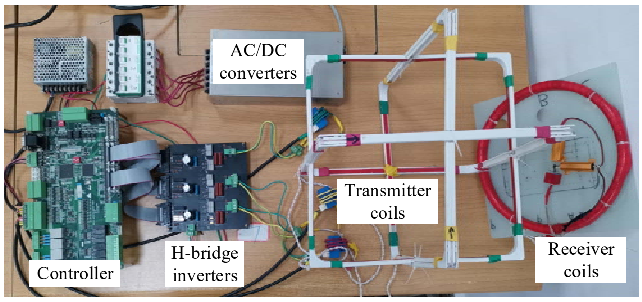

Fig. 5. 3D WPT system experimental prototype

The experimental prototype is mainly composed of the following parts: controller, current sampling circuit, inverter drive circuit, H-bridge inverter based on gallium nitride (GaN) devices, transmitting coil, and receiving coil. The schematic block diagram of the experimental platform is shown in Fig. 6. The controller uses a digital signal processor (DSP) TMS320F28335 and a field programmable gate array (FPGA)

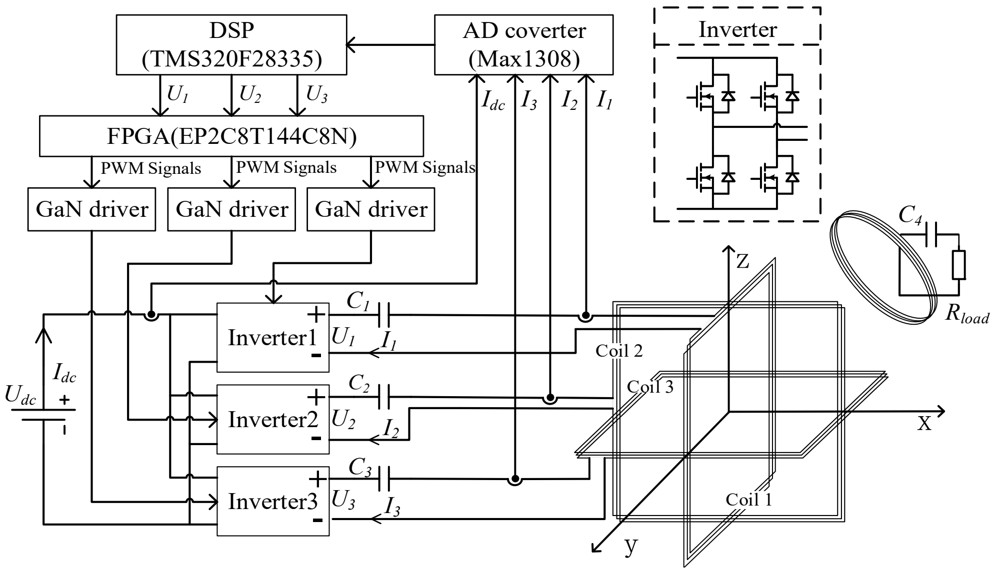

Fig. 6. Schematic block diagram of the 3D WPT system experimental prototype

EP2C8T144C8N. DSP is used for mathematical calculations and algorithm design. FPGA receives control signals from DSP and generates pulse width modulation (PWM) signals that drive the inverter. The current sampling circuit uses a current sensor HAS 50-S (LEM), and the output signal is conditioned by the operational amplifier circuit and converted into a digital signal by the Max1308 and transmitted to the controller for processing. The inverter uses GaN device GS61008T to form an H-bridge inverter circuit. The inverter uses a DC 12V voltage source to supply power. Three square coils are placed orthogonally to form the transmitting part. And the receiving coil is one circular coil. Each coil has a resonance compensation capacitor to make the system work in a fully resonant state. The system parameters are shown in Table I. The resonant frequency of the system is 20kHz. The execution cycle of the algorithm in the experimental prototype is 10ms. And the algorithm parameters are shown in Table II.

Table I
Actual parameters of the 3D WPT system

Symbol	Value	Symbol	Value	Symbol	Value
L_1	10.06μH	C_2	6.61μF	R_1	50.23 mΩ
L_2	10.09μH	C_2	6.59μF	R_2	50.30 mΩ
L_3	10.11μH	C_3	6.58μF	R_3	50.43 mΩ
L_4	101.28μH	C_4	0.66μF	R_4+R_{load}	0.63 Ω

Because the system uses a DC 12V voltage source for power supply, the DC side input current can be used to calculate the total input power of the system. After the DSP obtains the total input power of the system, a group of synthetic magnetic field vector angles can be obtained through the ESA based on square wave. Then the desired values of the three coil currents are obtained. When the coil current is stable, the current detection is carried out again. Then the control algorithm iteratively run until the maximum power transmission position is located. However, due to the existence of the detection signal of the ESA based on square wave, the actual system power is not the maximum after the system

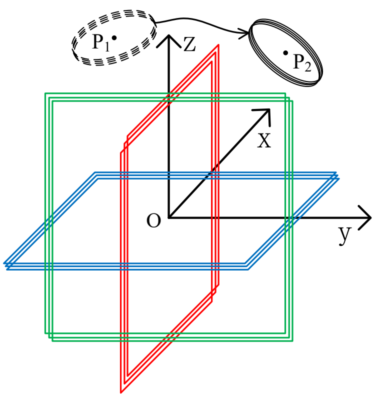

Fig. 7. Specific positions, orientations, and movement of the receiver coil in this experiment

Table II
Parameters of the proposed algorithm

Symbol	Value	Symbol	Value	Symbol	Value
I	8A	ω_1	157.07rad/s	ω_2	314.15rad/s
h_1	80rad/s	h_2	80rad/s	a_1	0.3
a_2	0.3	k_1	5	k_2	3

locates the maximum power transmission position. When the output of the integrator is less than a designed threshold value, the system will enter a stable state and the detection signal will be deleted. When the load position is judged to change, the ESA based on square wave runs again.

The steps of the experiment are shown in Fig. 7. First, place the load coil at the P_1 position, and point the synthesized magnetic field vector to the minimum power transmission position. Then let the 3D WPT system run with the ESA based on square wave. Observe the process of the system while is locating the maximum power transmission position. Then manually move the load coil to the P_2 position. Observe the process when the ESA based on square wave tracking the maximum power transmission position.

The overall experimental waveform of the system is shown in Fig. 8. I_1, I_2, I_3 are the current waveforms of the three coils. And I_{dc} is the input current of the DC power supply, which can represent the total power of the system. In region I, system works at the minimum power transmission position (perpendicular to the load position). Region III is the steady-state waveform at position P_1. The ESA starts to run in Region II, which is equivalent to a sudden change in the load position. During the running process of the ESA, θ and φ will tend to the maximum power transmission position. Thus, Region II is the process of locating the maximum power transmission position from the minimum power transmission position and the detection time is less than 150ms. The detailed waveform is shown in Fig. 9. It shows that the

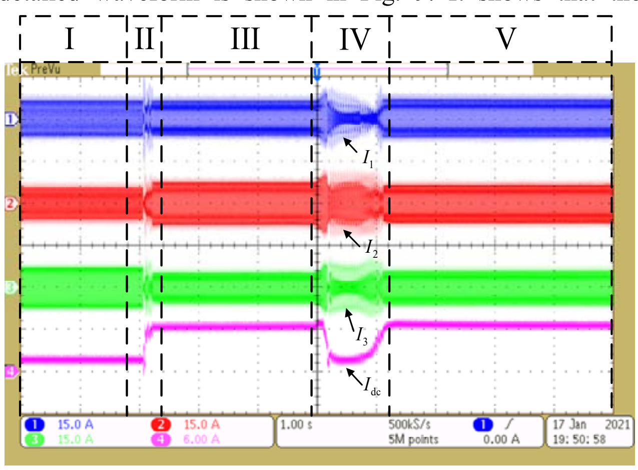

Fig. 8. Experimental waveforms of the ESA based on square wave

This article has been accepted for publication in a future issue of this journal, but has not been fully edited. Content may change prior to final publication. Citation information: DOI 10.1109/TIA.2021.3099777, IEEE Transactions on Industry Applications

maximum power transmission position can be found within 150ms. Region IV is the dynamic load tracking process when the load coil changes manually from position P_1 to position P_2. Region V is the steady state of the load coil at position P_2. The detailed steady-state waveforms of region I, region III, region V are shown in Fig. 10, Fig. 11, and Fig. 12, respectively.

The RMS values of the currents in Fig. 10, Fig. 11, and Fig. 12 are shown in Table III. According to Table III, the estimated value of the azimuth parameter obtained by the system in the first position is (-51.13°,-60.09°). And the estimated value of the azimuth parameter obtained by the system at the second position is (45.24°,57.61°). The position

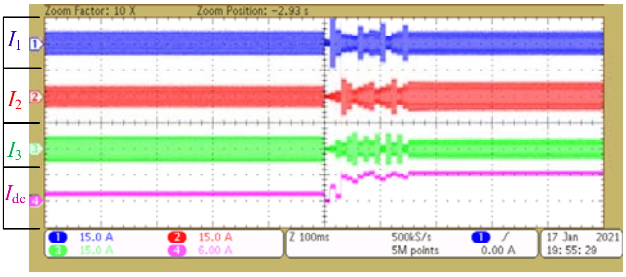

Fig. 9. The detailed steady-state waveforms of region II

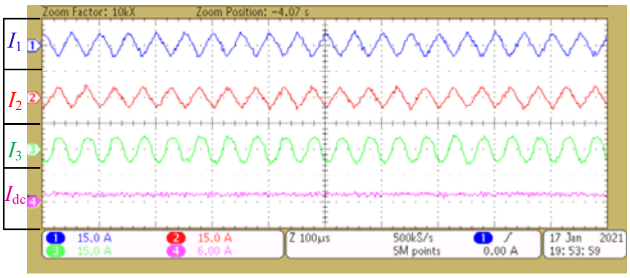

Fig. 10. The detailed steady-state waveforms of region I

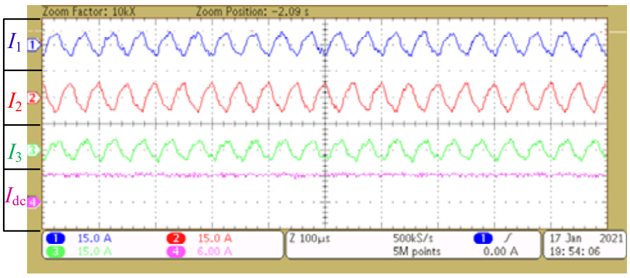

Fig. 11. The detailed steady-state waveforms of region III

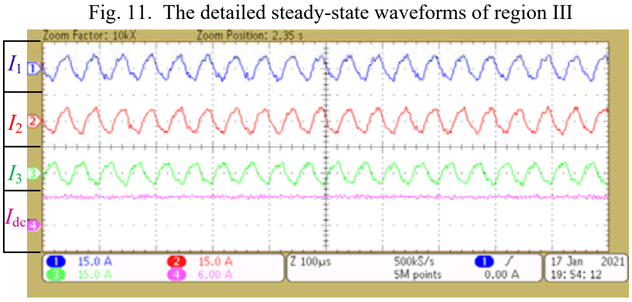

Fig. 12. The detailed steady-state waveforms of region V

Table III

The actual value of the current and its corresponding θ and φ

Region	I_1	I_2	I_3	θ	φ
I	4.1 (-)	3.72	5.49	-42.22°	45.24°
III	4.32 (-)	5.36	3.96 (-)	-51.13°	-60.09°
V	4.74 (-)	4.78 (-)	4.27	45.24°	57.61°

Note: "-" means the opposite current direction.

obtained by the system is basically the same as the position of the load coil in the actual system.

VI. Comparison and Discussion

A comparative study of different load tracking methods to realize maximum power transmission of the WPT system is shown in Table IV. Reference [21] proposed the mathematical method and the two-plane method for three-dimensional (3D) WPT system. The mathematical method is based on solving a system of equations to obtain the maximum power transmission point. And the two-plane method is based on a geometric solution to solve the maximum power transmission point. However, these two methods are computationally expensive and have poor real-time performance. Reference [23] proposed the parameter identification method and gradient descent method. The parameter identification method is approximate to the mathematical method, and the maximum power transmission point is also obtained by solving a system of equations. The gradient descent method first applied mathematical optimization algorithm to solve the load tracking problem, which greatly simplifies the calculation of load tracking in discrete systems. But this univariate gradient descent method is only suitable for 2D WPT system. Based on the polar coordinate system, reference [24] proposed a dual-angle gradient descent method, which is successfully applied in the 3D WPT system. But its multi-variable optimization process requires a step-by-step optimization, which is time-consuming. To further optimize this process, this paper proposes an extremum seeking algorithm based on square wave, which can realize the synchronization of the multi-variable optimization process.

VII. Conclusion

This paper proposes a control scheme based on the improved ESA for the 3D WPT system. The improved ESA uses the square wave signal instead of the sinusoidal signal as the detection signal, which reduces the computational complexity of the controller and make the system easy to be applied in practice. Moreover, the convergence of the ESA based on square wave is proved by analyzing the mathematical model of the system. An experimental prototype is built for verification. The experiment results manifest that

Table IV
Comparison with different control methods to achieve maximum power transmission

	[21]		[23]		[24]	This work
Method	Mathematical Method	2-Plane Method	Parameter Identification Method	Gradient Descent Method	3D gradient Descent Method	Extremum Seeking Algorithm
System Model	3D WPT system	3D WPT system	2D WPT system	2D WPT system	3D WPT system	3D WPT system
Method Type	Mathematical calculation	Geometric calculation	Mathematical calculation	Iterative optimization	Iterative optimization	Iterative optimization
Transmitting coil structure	Orthogonal circular coil	Orthogonal circular coil	Orthogonal square coil	Orthogonal square coil	Orthogonal square coil	Orthogonal square coil
Receiving coil quantity	One	One	One	One	Multiple	One
Tracking Speed	--	--	--	100ms	200ms	150ms
Algorithm complexity	Complex	Complex	Complex	Simple	Simple	Simple
Features	Computationally expensive, poor real-time performance	Computationally expensive, poor real-time performance	Computationally expensive, poor real-time performance	Univariate optimization	Multivariate step-by-step optimization	Multi-variable synchronous optimization

the system can track the load position smoothly when the load position changes manually. And the system can reach the maximum power transmission point within 150ms after the load position varies.

VIII. Appendix

The total input power of the system can be expressed as:

$$P_{in} = A + BC^2 \tag{A1}$$

where $A = I^2 R$, $B = \omega^2 I^2 (R_4 + R_{load}) / [(R_4 + R_{load})^2 + X_4{}^2]$, $C = M_{14}\sin\theta\cos\varphi + M_{24}\sin\theta\sin\varphi + M_{34}\cos\theta$.

The first-order partial derivatives of the above formula to θ and φ can be expressed as

$$\begin{aligned}\frac{\partial P_{in}}{\partial\theta} &= 2BC\frac{\partial C}{\partial\theta} \\ &= 2BC(M_{14}\cos\theta\cos\varphi + M_{24}\cos\theta\sin\varphi - M_{34}\sin\theta) \\ &= 2BCD\end{aligned} \tag{A2}$$

and

$$\begin{aligned}\frac{\partial P_{in}}{\partial\varphi} &= 2BC\frac{\partial C}{\partial\varphi} \\ &= 2BC(-M_{14}\sin\theta\sin\varphi + M_{24}\sin\theta\cos\varphi) \\ &= 2BCE\end{aligned} \tag{A3}$$

where

$$\begin{aligned}D &= M_{14}\cos\theta\cos\varphi + M_{24}\cos\theta\sin\varphi - M_{34}\sin\theta \\ &= \sqrt{\left(\sqrt{M_{14}{}^2 + M_{24}{}^2}\sin(\arctan\frac{M_{14}}{M_{24}} + \varphi)\right)^2 + M_{34}{}^2} \\ &\quad \times\sin\left(\arctan\frac{\sqrt{M_{14}{}^2 + M_{24}{}^2}\sin(\arctan\frac{M_{14}}{M_{24}} + \varphi)}{M_{34}} - \theta\right)\end{aligned} \tag{A4}$$

$$\begin{aligned}E &= -M_{14}\sin\theta\sin\varphi + M_{24}\sin\theta\cos\varphi \\ &= \sqrt{M_{14}{}^2 + M_{24}{}^2}\sin\theta\sin(\arctan\frac{M_{24}}{M_{14}} - \varphi)\end{aligned} \tag{A5}$$

The second order mixed partial derivative of the total input power with respect to θ and φ can be expressed as

$$\frac{\partial^2 P_{in}}{\partial\theta\,\partial\varphi} = 2B(\frac{\partial C}{\partial\varphi}D + C\frac{\partial D}{\partial\varphi}) \tag{A6}$$

$$\frac{\partial^2 P_{in}}{\partial\varphi\,\partial\theta} = 2B(\frac{\partial C}{\partial\theta}E + C\frac{\partial E}{\partial\theta}) \tag{A7}$$

where

$$\begin{aligned}\frac{\partial D}{\partial\varphi} = \frac{\partial E}{\partial\theta} &= -M_{14}\cos\theta\sin\varphi + M_{24}\cos\theta\cos\varphi \\ &= \sqrt{M_{14}{}^2 + M_{24}{}^2}\cos\theta\sin(\arctan\frac{M_{24}}{M_{14}} - \varphi)\end{aligned} \tag{A8}$$

When (A1) is at its maximum point, that is $\gamma_{3-D} + \theta = \pi/2$ or $3\pi/2$, $\arctan(M_{14}/M_{24}) + \varphi = \pi/2$ or $3\pi/2$. Therefore, the following formula can be obtained.

$$\theta = \arctan\frac{\sqrt{M_{14}{}^2 + M_{24}{}^2}\sin(\arctan\frac{M_{14}}{M_{24}} + \varphi)}{M_{34}} \tag{A9}$$

and

$$\varphi = \arctan\frac{M_{24}}{M_{14}} \tag{A10}$$

Substituting equations (A9) and (A10) into equations (A4), (A5) and (A8), the following equation can be obtained.

$$D = E = \frac{\partial D}{\partial \varphi} = \frac{\partial E}{\partial \theta} = 0 \tag{A11}$$

Because of $f(\theta,\varphi) = P_{in}$ and substituting equation (A11) into formula (A2), (A3), (A6) and (A7), the following equation can be obtained.

$$f_\theta{}' = f_\varphi{}' = f_{\theta\varphi}{}'' = f_{\varphi\theta}{}'' = 0 \tag{A12}$$

REFERENCE

[1]. N. Tesla, "High frequency oscillators for electro-therapeutic and other purposes," *Proceedings of the IEEE*, vol. 87, no. 7, pp. 1282-, July 1999.

[2]. G. A. Covic and J. T. Boys, "Inductive Power Transfer," *Proceedings of the IEEE*, vol. 101, no. 6, pp. 1276-1289, June 2013.

[3]. J. H. Kim et al., "Development of 1-MW Inductive Power Transfer System for a High-Speed Train," *IEEE Transactions on Industrial Electronics*, vol. 62, no. 10, pp. 6242-6250, Oct. 2015.

[4]. S. Sinha, A. Kumar, B. Regensburger and K. K. Afridi, "A New Design Approach to Mitigating the Effect of Parasitics in Capacitive Wireless Power Transfer Systems for Electric Vehicle Charging," *IEEE Transactions on Transportation Electrification*, vol. 5, no. 4, pp. 1040-1059, Dec. 2019.

[5]. M. Rozman et al., "Smart Wireless Power Transmission System for Autonomous EV Charging," *IEEE Access*, vol. 7, pp. 112240-112248, 2019, doi: 10.1109/ACCESS.2019.2912931.

[6]. V. Cirimele, M. Diana, F. Freschi and M. Mitolo, "Inductive Power Transfer for Automotive Applications: State-of-the-Art and Future Trends," *IEEE Transactions on Industry Applications*, vol. 54, no. 5, pp. 4069-4079, Sept.-Oct. 2018.

[7]. J. Zhu, Y. Ban, Y. Zhang, Z. Yan, R. Xu and C. C. Mi, "Three-Coil Wireless Charging System for Metal-Cover Smartphone Applications," *IEEE Transactions on Power Electronics*, vol. 35, no. 5, pp. 4847-4858, May 2020.

[8]. M. Manoufali, K. Bialkowski, B. Mohammed and A. Abbosh, "Wireless Power Link Based on Inductive Coupling for Brain Implantable Medical Devices," *IEEE Antennas and Wireless Propagation Letters*, vol. 17, no. 1, pp. 160-163, Jan. 2018.

[9]. Q. Wang, W. Che, M. Mongiardo and G. Monti, "Wireless Power Transfer System With High Misalignment Tolerance for Bio-Medical Implants," *IEEE Transactions on Circuits and Systems II: Express Briefs*, vol. 67, no. 12, pp. 3023-3027, Dec. 2020.

[10]. J. Zhou, P. Yao, Y. Chen, K. Guo, S. Hu and H. Sun, "Design Considerations for a Self-Latching Coupling Structure of Inductive Power Transfer for Autonomous Underwater Vehicle," *IEEE Transactions on Industry Applications*, vol. 57, no. 1, pp. 580-587, Jan.-Feb. 2021.

[11]. N. Kang, C. Ma and M. Liu, "A Linear Extendable Phase-shift Controlled Multi-coil Transmitter Architecture for Wireless Power Transfer with 3D Magnetic Field Shaping," in *Proc. 2020 IEEE PELS Workshop on Emerging Technologies: Wireless Power Transfer (WoW), Seoul, Korea (South),* 2020, pp. 170-177.

[12]. Y. Wu, H. Zhang, M. Liu, N. Kang and C. Ma, "Optimization of Super Capacitor Buffered Dynamic Wireless Power Transfer System," in *Proc. 2020 IEEE PELS Workshop on Emerging Technologies: Wireless Power Transfer (WoW), Seoul, Korea (South),* 2020, pp. 364-369.

[13]. C. Cheng, Z. Zhou, W. Li, Z. Deng and C. C. Mi, "A Power Relay System With Multiple Loads Using Asymmetrical Coil Design," *IEEE Transactions on Industrial Electronics*, vol. 68, no. 2, pp. 1188-1196, Feb. 2021.

[14]. F. Wen, X. Chu, Q. Li, R. Li, L. Liu and F. Jing, "Optimization on Three-Coil Long-Range and Dimension-Asymmetric Wireless Power Transfer System," *IEEE Transactions on Electromagnetic Compatibility*, vol. 62, no. 5, pp. 1859-1868, Oct. 2020.

[15]. Z. Zhang and B. Zhang, "Angular-Misalignment Insensitive Omnidirectional Wireless Power Transfer," *IEEE Transactions on Industrial Electronics*, vol. 67, no. 4, pp. 2755-2764, April 2020.

[16]. J. H. Kim et al., "Plane-Type Receiving Coil With Minimum Number of Coils for Omnidirectional Wireless Power Transfer," *IEEE Transactions on Power Electronics*, vol. 35, no. 6, pp. 6165-6174, June 2020.

[17]. J. Feng, Q. Li, F. C. Lee and M. Fu, "Transmitter Coils Design for Free-Positioning Omnidirectional Wireless Power Transfer System," *IEEE Transactions on Industrial Informatics*, vol. 15, no. 8, pp. 4656-4664, Aug. 2019.

[18]. N. Ha-Van and C. Seo, "Analytical and Experimental Investigations of Omnidirectional Wireless Power Transfer Using a Cubic Transmitter," *IEEE Transactions on Industrial Electronics*, vol. 65, no. 2, pp. 1358-1366, Feb. 2018.

[19]. M. Fu, T. Zhang, X. Zhu, P. C. Luk and C. Ma, "Compensation of Cross Coupling in Multiple-Receiver Wireless Power Transfer Systems," *IEEE Transactions on Industrial Informatics*, vol. 12, no. 2, pp. 474-482, April 2016.

[20]. D. Lin, C. Zhang and S. Y. R. Hui, "Mathematical Analysis of Omnidirectional Wireless Power Transfer—Part-I: Two-Dimensional Systems," *IEEE Transactions on Power Electronics*, vol. 32, no. 1, pp. 625-633, Jan. 2017.

[21]. D. Lin, C. Zhang and S. Y. R. Hui, "Mathematic Analysis of Omnidirectional Wireless Power Transfer—Part-II Three-Dimensional Systems," *IEEE Transactions on Power Electronics*, vol. 32, no. 1, pp. 613-624, Jan. 2017.

[22]. C. Zhang, D. Lin and S. Y. Hui, "Basic Control Principles of Omnidirectional Wireless Power Transfer," *IEEE Transactions on Power Electronics*, vol. 31, no. 7, pp. 5215-5227, July 2016.

[23]. M. Su, Z. Liu, Q. Zhu and A. P. Hu, "Study of Maximum Power Delivery to Movable Device in Omnidirectional Wireless Power Transfer System," *IEEE Access*, vol. 6, pp. 76153-76164, 2018.

[24]. W. Tang, Q. Zhu, J. Yang, D. Song, M. Su and R. Zou, "Simultaneous 3-D Wireless Power Transfer to Multiple Moving Devices With Different Power Demands," *IEEE Transactions on Power Electronics*, vol. 35, no. 5, pp. 4533-4546, May 2020.

[25]. G. C. Santos and T. R. Oliveira, "Gradient Extremum Seeking With Nonconstant Delays," *IEEE Access*, vol. 8, pp. 120429-120446, 2020.

[26]. T. R. Oliveira, J. Feiling, S. Koga and M. Krstić, "Multivariable Extremum Seeking for PDE Dynamic Systems," *IEEE Transactions on Automatic Control*, vol. 65, no. 11, pp. 4949-4956, Nov. 2020.

[27]. X. Liu et al., "Novel Dual-Phase-Shift Control With Bidirectional Inner Phase Shifts for a Dual-Active-Bridge Converter Having Low Surge Current and Stable Power Control," in IEEE Transactions on Power Electronics, vol. 32, no. 5, pp. 4095-4106, May 2017.